THE JOURNAL OF PHYSICAL CHEMISTRY A

 VOLUME 106, NUMBER 4, JANUARY 31, 2002

ARTICLES

Visible to Near-Infrared Ultrafast Spectroscopy of a Quasi-One-Dimensional Halogen-Bridged Mixed-Valence Metal Complex $[Pt(en)_2][Pt(en)_2Cl_2](ClO_4)_4$

Atsushi Sugita,[†] Tomoshige Furuhi,[†] Masahiro Yamashita,[‡] and Takayoshi Kobayashi*,[†]

Department of Physics, University of Tokyo, 7-3-1 Hongo, Bunkyo-ku, Tokyo, 113-0033 Japan, and Department of Chemistry, Tokyo Metropolitan University, Hachioji, Tokyo, 192-0397 Japan

Received: October 5, 2000; In Final Form: November 12, 2001

Ultrafast relaxation dynamics is studied in a quasi-one-dimensional halogen-bridged mixed-valence metal complex $[Pt(en)_2][Pt(en)_2Cl_2](ClO_4)_4$ by pump−probe spectroscopy. A photoinduced absorption spectrum is measured in a broadband energy region of 0.6−2.6 eV, applying optical parametric amplification. The measurement is performed at both 293 and 4 K. The photoinduced absorption spectrum consists of the three contributions with different time and temperature dependence. One is the absorption band ascribed to the self-trapped exciton (STE), and the second is that due to the spatially uncorrelated neutral-soliton pair. Just after the photoexcitation, the STE is in a nonequilibrium state, and the time required for the thermalization is evaluated to be about 1 ps. The formation time of the third one is coincident with the thermalization time of the STE, and it is attributed to the spatially confined neutral-soliton pair.

1. Introduction

Optical, electronic, and transport properties are attracting a lot of interests in quasi-one-dimensional materials,[1,2] such as π-conjugated organic polymers,[3−6] J aggregates of organic molecules,[7,8] or one-dimensional metal complexes,[9−10] because of strong electron or exciton confinement in such materials. Quasi-one-dimensional halogen-bridged mixed-valence metal complexes (HMMCs) also belong to such a group of compounds, and several properties based on charge-transfer (CT) excitons have been studied both experimentally and theoretically.[11−18] The chemical formula of HMMC is expressed as $[M(AA)_2][M(AA)_2X_2]Y_4$. Here, M, X, AA, and Y are the transition metal ion, the bridged-halogen ion, the ligand molecule, and the counterion, respectively. The one-dimensional chain of HMMC consists of alternate transition metal ions with a valence +3 (M^{3+}) and bridged-halogen ions with a valence −1 (X^-). The complex is characterized by strong electron−phonon coupling. The distribution of the electron on an MX chain, hence, forms a charge density wave (CDW) ground state because of a Peierls transition, which is expressed as

$$-X^-\cdots M^{3-\rho}\cdots X^- - M^{3+\rho} - X^-\cdots M^{3-\rho}\cdots X^- - M^{3+\rho} - X^-\cdots$$

There is an inequality of the amount of charge distribution between neighboring transition-metal sites, and the metal ions $M^{3+\rho}$ and $M^{3-\rho}$ are arrayed alternately on a quasi-one-dimensional line, defining the quantity of charge transfer as ρ. Accordingly, the bridged-halogen ion X^- with a negative charge is shifted from a position halfway between $M^{3+\rho}$ and $M^{3-\rho}$, and it is placed closer to the $M^{3+\rho}$ ion. The strong electron−phonon coupling effect in HMMC is confirmed by the large Stokes shift of the fluorescence spectrum and the observation of higher order overtones in the Raman scattering signal.[19]

A lot of attention has been paid to the formation and relaxation dynamics of the photoexcited states, and they

* To whom correspondence should be addressed. E-mail: kobayashi@phys.s.u-tokyo.ac.jp. Fax: +81-3-5841-4240.
[†] University of Tokyo.
[‡] Tokyo Metropolitan University.

10.1021/jp003651q CCC: $22.00
Published on Web 01/08/2002

have been extensively studied both experimentally[20−27] and theoretically.[28−32] The stationary absorption is observed in a visible to near-infrared region depending on constituent M, X, AA, and Y, and it is attributed to a CT-exciton band.[11,12] The CT-free exciton is expected to be unstable by itself, and it geometrically relaxes to the more stable localized state, that is, a self-trapped exciton (STE) state. This is because there is no potential barrier between the free exciton and the STE states, which is a characteristic feature common to one-dimensional systems.[1,2,32] The formation of the STE in the HMMC system has been confirmed by an unusually large Stokes shift of the fluorescence signal extending almost half of the excitonic transition energy.[19,33] However, the STE state is not the most stable excited state, and it has a nonradiative relaxation channel to a neutral-soliton state, that is, one kind of nonlinear excitation.[25−27] The formation of other nonlinear excitations, that is, charged-soliton and polaron, were also reported[21,25,26]. They are generated not from the STE but from the lattice relaxation of the unbound electron−hole pair.

The relaxation dynamics of the exciton states and nonlinear excitations were extensively studied in π-conjugated polymers.[3−6] The decay rates of these transient states were found to be much slower in HMMC than those in π-conjugated polymers.[20−24] In HMMC, the electron−phonon coupling is considered to have the same order of the magnitude as the transfer energy, whereas the transfer energy is much larger than the electron−phonon coupling in conjugated polymers. Therefore, the excited states are bound more tightly to the lattice in HMMC than in conjugated polymers. Recently, the dynamics of these transient states were studied in the femtosecond and picosecond time regions, and it was reported that some of the photoinduced states show an ultrafast optical response.[33−39]

The time-resolved fluorescence signal was measured with an up-conversion method on $[Pt(en)_2][Pt(en)_2Cl_2](ClO_4)_4$ (en = ehtylenediamine). The rapidly decaying fluorescence signal is observed, in addition to the slowly decaying fluorescence signal because of the STE with the lifetime of about 100 ps.[36,37] The time constant of the rapidly decaying signal was about 1 ps, and it is dependent on the probe photon energy. This fluorescence signal is attributed to the nonequilibrated STE, and the decay time is correspondent to the process of dissipating an excess vibrational energy. We also studied the other HMMC compound of $[Pt(en)_2][Pt(en)_2Br_2](ClO_4)_4$ with femtosecond time-resolved absorption spectroscopy.[39] The formations of two kinds of soliton pairs with different kinetics are observed; one is a spatially confined neutral-soliton pair, and the other is a spatially uncorrelated neutral-soliton pair.

In the present paper, the ultrafast relaxation dynamics of the photoexcited states are studied for $[Pt(en)_2][Pt(en)_2Cl_2](ClO_4)_4$ (hereafter abbreviated as Pt−Cl). The time-resolved absorption spectrum is measured with pump−probe absorption spectroscopy. A broadband near-infrared pulse is employed as a probe in addition to a white light continuum generated by the self-phase modulation (SPM). The observable spectral region is very broad, extending from 0.6 to 2.6 eV. The photoinduced absorption spectrum consists of three contributions with different time and temperature dependence, that is, self-trapped exciton, spatially uncorrelated neutral-soliton pair, and the spatially confined neutral-soliton pair. The formation, the relaxation, and the transport properties of these transient states are to be discussed in detail.

2. Experimental Section

The single crystal of Pt−Cl is synthesized by the method previously reported.[40] Additionally, an oriented thin film is prepared on a CaF_2 substrate for the measurement of the absorption spectrum.[41]

The time-resolved absorption spectrum is studied by pump−probe spectroscopy. Femtosecond pulses are generated by an Er-doped fiber laser which is pumped by an all-solid-state CW laser composed of a master-oscillator power amplifier (MOPA; ErF femtosecond fiber laser, Clark-MXR).[42] The pulse width, center wavelength, and average output energy of the laser at 34 MHz repetition rate are 150 fs, 1.55 μm, and 50 mW. The pulses are frequency-doubled by a β-BaB_2O_4 (BBO) crystal, and the second harmonics (0.775 μm, 150 fs, and 5 mW) is employed as the seed in a Ti:sapphire regenerative amplifier (CPA-1000, Clark-MXR) pumped by the second harmonics from a Q-switched Nd:YAG (yttrium−aluminum−garnet) laser (0.532 μm, 5 mJ). The pulse width and the average energy of the amplified pulse at a 100 Hz repetition rate are 160 fs and 0.5 mJ, respectively.

The excitation pulse is the second harmonics (0.388 μm) of the amplified pulse generated in an LiB_3O_5 (LBO) crystal. The probe light spectrum extends over a broadband wavelength range between 0.48 and 2.10 μm. A femtosecond white light continuum is available at the wavelengths shorter than 1.6 μm, generated by SPM in a 10 mm cell containing CCl_4. Probe light with wavelengths longer than 1.6 μm is generated in a parametric mixing process. The detail of the difference frequency generation (DFG) has been already reported elsewhere[43] and here only briefly described. The pump for the parametric process (ω_p) is the fundamental of the Ti:sapphire laser at 0.775 μm. The signal light (ω_s) is the near-infrared part of the white light continuum at wavelengths of 1.2−1.5 μm. Both the pump and signal pulses are combined collinearly by a dichroic mirror and focused into a $KTiOPO_4$ (KTP) crystal to generate an idler pulse with the difference frequency of pump and signal pulses ($\omega_i = \omega_p + \omega_s$). The KTP crystal is cut at $\theta = 38.8°$ and $\phi = 90°$ for type-II phase matching (o = e + o) in the $y-z$ plane. The wavelength of the idler pulse can be tuned by rotating the crystal angle. The bandwidth of the idler pulse is 700−800 cm^{-1}.

The excitation and probe pulses are focused on the sample with spot sizes of about 0.3 and 0.2 mm, respectively. The density of the excitation photon is estimated to be about 1.0×10^{16} photons/cm^2. The MX chains are well aligned, and the polarizations of the pump and probe pulses are parallel to the orientation of the MX chains. For the wavelength region of 0.5−1.2 μm, both probe and reference pulses are dispersed in a polychromator and multichannel photodiode array detectors (ST-1000, Princeton Instruments) detect these two beams. For the wavelength region longer than 1.2 μm, each pulse is measured by a set of polychromators and liquid-nitrogen-cooled platinum silicon (PtSi) multichannel detectors (EG&G Reticon, RH1024SIU). The temporal characteristic of the probe beam is measured by the cross-correlation method, which is used to correct the group delay dispersion. The time resolution of the total system is determined to be about 300 fs in the whole probe spectral range studied. The experiments are performed at both 293 and 4 K.

3. Results

Figure 1a shows the stationary reflection spectrum of a thin film sample of Pt−Cl at 293 K. The spectrum is dichroic, namely, it depends on the polarization of the light. Both parallel and perpendicular spectra are essentially the same as those of a single crystal of Pt−Cl in the literature.[11,12] The stationary spectrum is transformed from the reflection spectrum in Figure

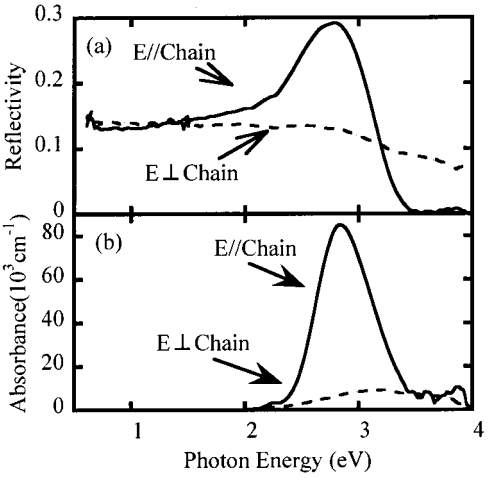

Figure 1. (a) Stationary reflection spectrum of Pt−Cl at 293 K. The solid and dashed curves show the spectra with the polarizations of the light parallel and perpendicular to the MX chain, respectively. (b) Stationary absorption spectrum of Pt−Cl at 293 K. The spectrum is transformed from the stationary reflection spectrum using the Kramers−Kronig relation. The solid and dashed curves show the spectra with the polarization of the light parallel and perpendicular, respectively, to the MX chain.

1a using the Kramers−Kronig relations, because the sample thickness of about 1 μm is too thick to measure the stationary absorption spectrum correctly. The Roessler correction method is applied,[44] because of the limitation in the observed photon energy region. Figure 1b shows the stationary absorption spectrum of Pt−Cl. In the configuration of the light polarization parallel to the MX chain, the absorption spectrum has a peak at 2.7 eV, and the spectrum shape is asymmetric with a tail in the higher energy region. According to the previous results, the absorption band is attributed to the CT exciton band.[11,12] On the other hand, no significant absorption signal is found for perpendicular polarization to the MX chain. This indicates that the interchain transition of an electron does not take place, because of the large separation between neighboring MX chains. Therefore, the transport of an electron or an exciton is considered to be restricted to the direction along the MX chain in the present thin film sample, in the same way as in a single crystal.

Figure 2 shows a time-resolved photoinduced absorption (PA) spectrum of Pt−Cl at 293 K. Both the polarizations of the excitation and probe are both parallel to the MX chain. The excitation photon energy of 3.2 eV is higher than the peak photon energy of the CT-exciton band. Consequently, the photoexcitation induces the transition to higher vibrational levels in the CT-exciton band. At the fundamental probe energy of the Ti:sapphire laser extending from 1.51 to 1.68 eV, the background, because of continuous amplified stimulated emission (ASE), prevents a proper time-resolved measurement of the PA spectrum. Therefore, the spectrum is interpolated with dashed lines in the energy region in Figure 2.

At an early stage after the photoexcitation, the PA spectrum has three peaks at almost 1.3, 2.2, and 2.5 eV, respectively (Figure 2 parts a and b). As the delay time is longer, the absorption band around 1.3 eV is found to disappear as seen in Figure 2 parts c and d. On the other hand, the other two peaks at 2.2 and 2.5 eV are still distinguished, and furthermore, the PA spectrum has another peak around 1.5 eV, which is not clearly seen at the earlier delay times (Figure 2e). The spectrum shape with these three peaks does not change substantially at the delay times longer than 20 ps. As another characteristic, the rise of the PA signal is found not to be instantaneous around

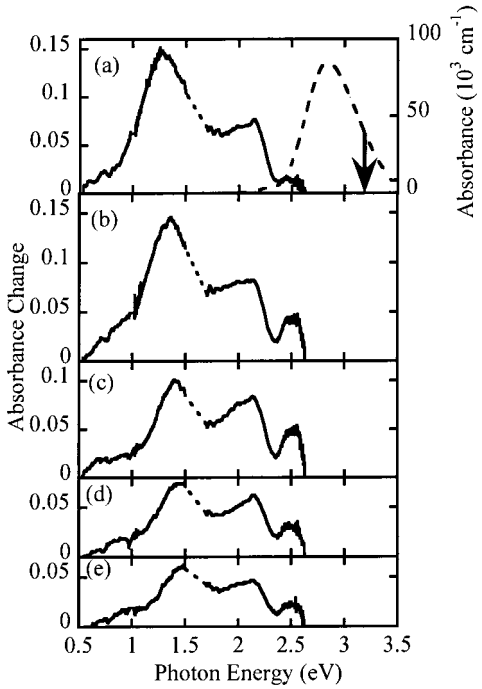

Figure 2. Time-resolved PA spectrum of Pt−Cl at the delay time of (a) 0.2, (b) 1.0, (c) 2.0, (d) 5.0, and (e) 20 ps (solid curves) at 293 K. The excitation energy is 3.2 eV, and an arrow denotes it. The excitation density is about 1.0×10^{16} photons/cm^2. The stationary absorption spectrum is also shown by a dashed curve at the top column.

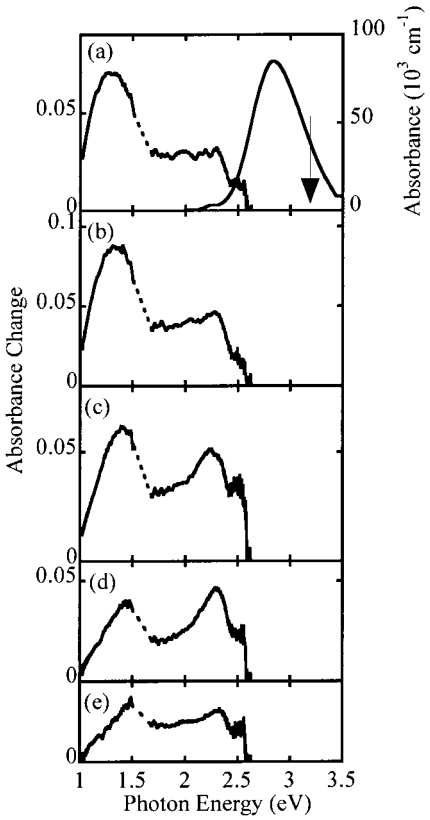

Figure 3. Time-resolved PA spectrum of Pt−Cl at the delay time of (a) 0.2, (b) 1.0, (c) 2.0, (d) 5.0, and (e) 20 ps (solid curves) at 4 K. The excitation energy is 3.2 eV, as shown by the arrow. The excitation density is about 1.0×10^{16} photons/cm^2. The stationary absorption spectrum at 293 K is also shown by a dashed curve.

2.2 eV, and it is a bit late after the photoexcitation. Figure 3 is the time-resolved PA spectrum of Pt−Cl at 4 K. As above-

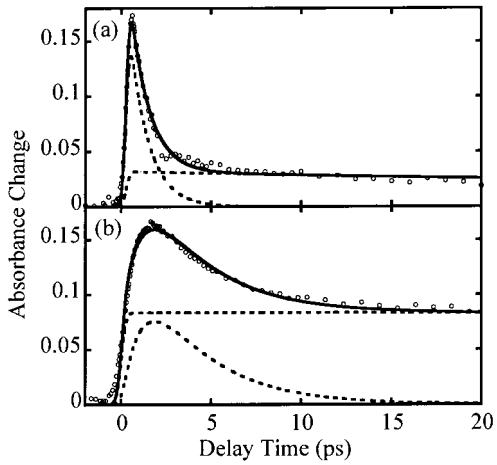

Figure 4. Time-dependence of the PA intensity of Pt−Cl probed at (a) 1.20 and (b) 2.20 eV at delay times shorter than 20 ps. The excitation energy is 3.2 eV, and the temperature is 293 K. Open circles denote the experimental data. The time-dependences a and b are fitted to eqs 1 and 2, respectively (solid curves). The components in each equation are also shown by dashed curves.

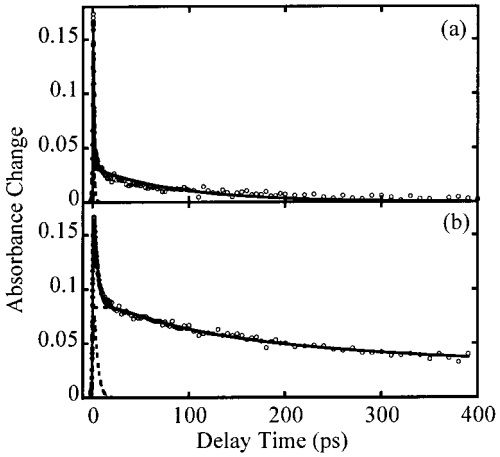

Figure 5. Same as Figure 3 but at delay times up to 400 ps.

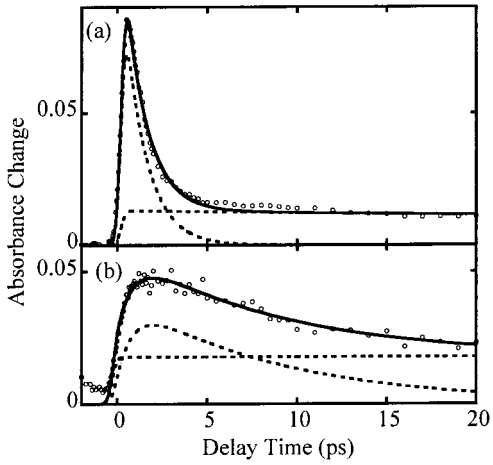

Figure 6. Time-dependence of the PA intensity of Pt−Cl probed at (a) 1.20 and (b) 2.20 eV, respectively, at delay times shorter than 20 ps. The excitation energy is 3.2 eV, and the temperature is 4 K. Open circles denote the experimental data. The time-dependence a and b is fitted to eqs 1 and 2, respectively (solid curves). The magnitudes of the terms in each equation are also shown by dashed curves.

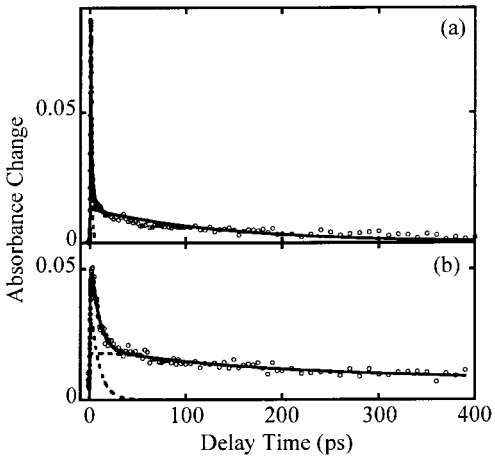

Figure 7. Same as Figure 6 but at delay times up to 400 ps.

mentioned, the PA spectrum cannot be measured correctly between 1.51 and 1.68 eV because of the ASE background in the white light continuum, and the spectrum is, therefore, interpolated in that region. The several spectroscopic features at 293 K are commonly observed at 4 K. In the previous work, Kanner et al. reported the photoinduced absorption spectrum of Pt−Cl in the subpicosecond time scale.[38] They measured the absorption spectrum with the several excitation photon energies lower and higher than the CT-exciton band. However, the corresponding PA band with a peak around 1.3 eV was not observed with any excitation energy.

Figures 4 and 5 show the time-dependence of the PA intensity at the delay times shorter than 20 and 400 ps, respectively. The probe photon energies are 1.20, 1.70, and 2.20 eV, and the temperature is 293 K. The time dependence at 4 K is also shown at the same photon energies in Figures 6 and 7. The temporal profiles at 1.20 eV (Figures 4a and 5a for 293 K and Figures 6a and 7a for 4 K) are expressed with the biexponential function as

$$\Delta A(t) = A \exp\left(-\frac{t}{\tau_A}\right) + B \exp\left(-\frac{t}{\tau_B}\right) \qquad (1)$$

The decay time constants are determined to be $\tau_A = 1.0 \pm 0.1$ ps and $\tau_B = 90 \pm 6$ ps at 293 K as a result of the least-squares fitting of the experimental data to eq 1. They are also determined as $\tau_A = 1.0 \pm 0.2$ ps and $\tau_B = 140 \pm 10$ ps at 4 K.

On the other hand, the time dependence at 2.20 eV is also shown at both of the temperatures (Figures 3b and 4b for 293 K and Figures 5b and 6b for 4 K). In both cases, the temporal profiles of the PA signals are reproduced with a relation described by eq 2:

$$\Delta A(t) = C\left[\exp\left(-\frac{t}{\tau_{C1}}\right) - \exp\left(-\frac{t}{\tau_{C2}}\right)\right] + \mathrm{D}\ \mathrm{erf}\left[\left(\frac{t}{T_D}\right)^{-1/2}\right] \qquad (2)$$

Here, erf() is an error function. The parameters are evaluated by a least-squares fitting as $\tau_{C1} = 3.4 \pm 0.6$ ps, $\tau_{C2} = 1.1 \pm 0.2$ ps, and $T_D = 68 \pm 8$ ps for 293 K and $\tau_{C1} = 8.8 \pm 0.4$ ps, $\tau_{C2} = 0.9 \pm 0.1$ ps, and $T_D = 91 \pm 10$ ps for 4 K. The first term in eq 2 expresses the PA component that increases with a rise time constant of τ_{C1}, and decreases with the decay time constant of τ_{C2}. The rise time τ_{C2} is in a good agreement within an experimental error at both of the temperatures, whereas the decay time τ_{C1} has clear temperature dependence, and it is 2.6 times larger at 4 K than at 293 K.

The second term erf$[(t/T_D)^{-1/2}]$ expresses the geminate recombination process of pair excited species that move by diffusion along a one-dimensional chain.[6,45] The pair excited species walk randomly along the one-dimensional chain, and

TABLE 1: Probe Energy Dependence of the Decay Time Constant τ_A at 293 and 4 K

photon energy (eV)	decay time constant τ_A at 293 K	decay time constant τ_A at 4 K
0.7	460 ± 20 fs	
0.9	620 ± 30 fs	
1.0	800 ± 40 fs	870 ± 30 fs
1.1	970 ± 30 fs	910 ± 50 fs
1.2	1.1 ± 0.1 ps	1.1 ± 0.2 ps
1.3	1.2 ± 0.2 ps	1.3 ± 0.2 ps

they disappear when they meet with each other. As for the formation of these pair species, the rise of the PA signal is instantaneous within 300 fs, the time resolution of the spectrometer. This means that the free CT excitons are decomposed into the pair excited species soon after the photoexcitation and that the pair species transport coherently along the MX chain until they begin the random walk. The time constant T_D is related to the diffusion constant, d, and the separation between two species, I_0, just after the decomposition from the CT exciton:

$$T_D = \frac{I_0^2}{4d} \tag{3}$$

It should be noted that the function $\mathrm{erf}[(t/T_D)^{-1/2}]$ is the solution of the diffusion equation in a continuous limit, although the real one-dimensional chain is divided into segmental areas by the metal sites and the excited species hop between the neighboring segments with a finite probability. However, this approximated equation is often used for analyzing the geminate recombination process, and it can reproduce the experimental results sufficiently well[6,46,47]. Shank et al. calculated numerically the diffusion equation where the pair species jump between the segments.[46] They pointed out that the approximated equation solved in the continuous limit is in a good agreement with the equation solved numerically in all of the delay time.

At other probe photon energies, the time dependence of PA can be reproduced with a combination of the four components constituting eqs 1 and 2, that is, the τ_A-decay component A, the τ_B-decay component B, the τ_{C2}-rise and τ_{C1}-decay component C, and the component D which decreases following the model of the geminate recombination process. There is no significant difference seen concerning the distribution of these four spectral components between 293 and 4 K. The components A and B are seen at the probe energy lower than 1.8 eV, whereas the component C is distributed mainly at the energy higher than 1.9 eV. The component D is distributed between 1.3 and 2.6 eV, and the specific three peaks at 1.5, 2.2, and 2.5 eV belong to this component. In Table 1, the probe energy dependence of τ_A is listed at several probe photon energies at both of the temperatures. The tendency is found that the constant τ_A gets longer, as the probe photon energy is higher.

4. Discussion

First, the relaxation dynamics of the τ_A- and τ_B-decay components are to be discussed. The time constant τ_A for the rapidly decaying component is about 1 ps, and it gets longer as the probe photon energy gets higher. There is no significant difference in the quantity τ_A between the two temperatures of 293 and 4 K, while the longer time constant τ_B is temperature-dependent. It is $\tau_B = 90 \pm 10$ ps at 293 K, and it increases to $\tau_B = 140 \pm 20$ ps at 4 K.

In the previous work, two fluorescence signals have been reported for Pt−Cl.[33,36,37] The first one is the emission due to the transition from the thermal STE level to the electronic ground state. The fluorescence lifetime depends on temperature, and it is about 70 ps at 293 K and 200 ps at 4 K.[33] The second signal is observed in a photon energy region higher than that of the slowly decreasing fluorescence signal.[36,37] The lifetime was reported to be 260 fs to 1.2 ps, depending on the probe photon energy, and it becomes longer as the probe photon energy gets larger. This rapidly decreasing signal is attributed to the emission from the STEs in the thermally nonequilibrated state. Namely, the nonthermal STEs are distributed over nonequilibrated excited vibrational states. The decay time constants of the rapidly and slowly decaying components are fairly in good agreement with those of the two STEs. Hence, it is concluded that the rapidly and slowly decaying components are attributed to the nonthermal and thermal STEs, respectively.

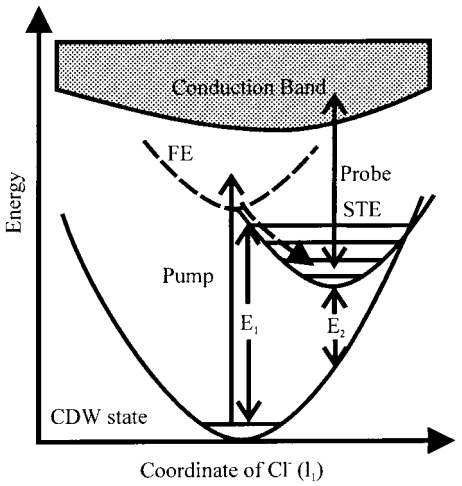

Figure 8. Model of the relaxation dynamics of the STE in Pt−Cl. The adiabatic potential curves are depicted as the function of coordinate of the chloride ion (l_1). E_1: the peak photon energy of absorption due to the free exciton. E_2: the peak photon energy of the fluorescence due to the STE.

The observed probe energy dependence of the time constant τ_A reflects the thermalization mechanism of the STE. Just after the formation, the STE is considered to be in a nonthermal distribution determined by the absorption cross section and laser spectrum, and it is concentrated around higher vibrational levels. Then, the nonthermal STE dissipates the excess vibrational energy and relaxes to lower vibrational levels described by the thermal statistics. Hence, the thermalization of the STE takes place from higher to lower vibrational levels. The PA due to STE is attributed to the transition from the exciton level to the conduction band (Figure 8). The PA signal observed at the lower probe energies, therefore, corresponds to the transition from the initial states of higher vibrational levels. Consequently, the PA signal at lower energies is expected to decrease faster than that with the higher energies.

The following two physical quantities are calculated for the time-resolved PA spectrum at each delay time to evaluate the spectral shift and the population change of the STE:

$$S(t) = \int_{E_1}^{E_2} \Delta A(t)\, \mathrm{d}E = fn\frac{\pi e^2 l}{mc \ln 10} \tag{4}$$

$$M(t) = \int_{E_1}^{E_2} \Delta A(t)\, E\, \mathrm{d}E/S(t) \tag{5}$$

Here, the integration is carried out over the photon energy E between $E_1 = 0.60$ eV and $E_2 = 1.51$ eV, where the PA spectrum is contributed mainly from the components A and B. The parameters f, n, l, m, e, and c are the probe photon energy,

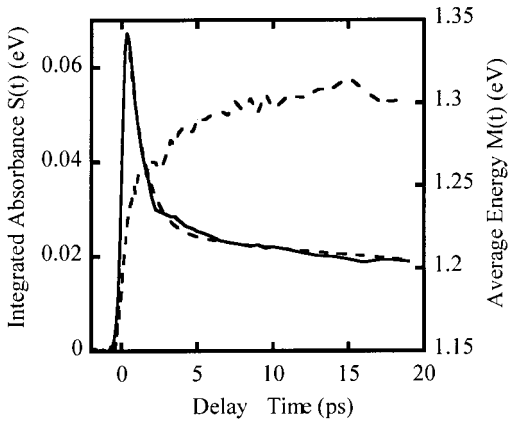

Figure 9. Time dependence of the integrated absorbance $S(t)$ (solid curve) and average probe photon energy $M(t)$ (dashed curve) of the PA band due to the STE. The temperature is 293 K. The time dependence of $S(t)$ is fitted to eq 6 and shown by dashed curve.

the oscillator strength, the population density of the STE, the sample thickness, electron mass, electronic charge and light velocity, respectively. When the oscillator strength does not change during the thermalization process, $S(t)$ depends only on the population density n. Hence, the change of $S(t)$ indicates the population change of the STE during the thermalization process. The second quantity $M(t)$ is the first-order momentum of the PA spectrum, that is, the average photon energy of the PA spectrum at the delay time t.

Figure 9 shows the time dependence of $S(t)$ and $M(t)$ up to 10 ps after photoexcitation at 293 K. The average energy $M(t)$ of the PA increases from 1.16 eV at 0 ps to 1.29 eV at 5 ps. As mentioned above, the PA because of the exciton corresponds to the transition from the STE levels to the conduction band. The shift of the average PA spectrum reflects the population redistribution of the nonthermal STE from higher to lower vibrational levels. On the other hand, the population change of the STE is evaluated from the integrated absorbance. The observed time dependence of $S(t)$ can be reproduced by the following equation:

$$S(t) = S_A \exp\left(-\frac{t}{\tau_A}\right) + S_B\left[\exp\left(-\frac{t}{\tau_B}\right) - \exp\left(-\frac{t}{\tau_A}\right)\right] \quad (6)$$

The equation indicates that the nonthermal STEs relax to the thermal STEs with the rate $1/\tau_A$ and, successively the thermal STEs relax to the electronic ground state with the rate $1/\tau_B$. The parameters are evaluated by the least-squares fitting as $\tau_A = 880 \pm 60$ fs and $S_A = (8.4 \pm 0.1) \times 10^{-2}$ eV for the nonthermal STE and $\tau_B = 85 \pm 6$ fs and $S_B = (2.5 \pm 0.1) \times 10^{-2}$ eV for the nonthermal STE. The quantity $S_B/S_A = 0.30$ corresponds to the probability that the nonthermal STE relaxes to the thermal distribution. The other 70% of the nonthermal STE relaxes to a state other than the thermal STE. During the thermalization process, the average energy reduces from $M(t = 0$ fs$) = 1.16$ eV to $M(t = 880$ fs$) = 1.25$ eV. Hence, the energy relaxation rate is estimated to be 102 meV/ps.

As has been reported in previous work, the fluorescence quantum efficiency of the thermal STE is 3%,[33] and the population decrease of the nonthermal STE through the radiative decay channel is negligibly small, because the fluorescence quantum efficiencies of the nonthermal and thermal STEs are expected to be of the same order.[36] The most probable relaxation path of the nonthermal STE is the relaxation channel to the component C, because the rise time $\tau_{C2} = 1.0$ ps at 293 K and $\tau_{C2} = 0.9$ ps at 4 K agrees well with the thermalization time of $\tau_A = 880$ fs defined in eq 6. The dynamic and spectroscopic properties of the component C will be later discussed.

Second, the dynamics of the component D is reported, whose time dependence is described with the function $\mathrm{erf}[(t/T_D)^{-1/2}]$ in eq 2. The function is the solution of the one-dimensional diffusion equation, and it expresses the geminate recombination process where the pair excited species walk randomly along the one-dimensional chain and disappear when they meet. In addition to it, the spectrum of the component C has three specific peaks at around 1.5, 2.2, and 2.5 eV. The spectral shape is well correspondent to the photoinduced absorption band ascribed to the neutral-soliton state reported in the previous work of Pt−Cl.[20] The spectrum had two characteristic peaks around 1.6 and 2.0 eV, and the absorption edge was 1.4 eV. The PA spectrum with these two specific peaks was commonly observed in other HMMCs, and the third peak was also observed in the energy region higher than the former two peaks in some of the HMMCs.[26,48] When the neutral solitons are generated photolytically, they should be formed as pair species, that is, the soliton and anti-soliton because of the conservation of the charges and spins within the MX chain before and after the photoexcitation. Consequently, they should disappear through the geminate recombination process. These observations support the assignment that the component C is attributed to the neutral soliton pair.

In the present experimental results, the time constant T_C is dependent on the temperature, and it is larger at 4 K than that at 293 K; that is, $T_C = 68 \pm 8$ ps at 293 K and 91 ± 10 ps at 4K. As can be seen in eq 3, the time constant T_C is determined by the two elements, that is, the parameters d for the diffusion constant and I_0 for the initial separation between soliton and anti-soliton pair. Among them, the initial pair separation I_0 is expected to be independent of the temperature from the following reason. As mentioned above, the formation time of the corresponding PA is faster than the temporal resolution of 300 fs at both 293 and 4 K, which suggests that the photogenerated CT exciton is decomposed into the soliton and anti-soliton pair just after the formation and they propagate coherently along the MX chain until they walk randomly (Figures 4c and 6c). The coherent propagation is driven by the sufficiently large excess vibrational energy, irrespective of the temperature. Thus, the temperature dependence of the time constant T_C is related to only the diffusion constant d.

Two factors determine the diffusion constant between the neighboring metal sites: one is the transfer energy, and the other is the electron−phonon coupling.[22] The charges are transferred between the neighboring metal ions by way of the bridged-halogen ion, and the quantity of the transfer energy is closely related with the overlap between the d_{z^2} orbital in the metal ions and the p_z orbital in the bridged-halogen ions.[11] This quantity is not dependent on the temperature of the system. On the other hand, the charge can be trapped by the local deformation of the lattice by the strong electron−phonon coupling. When the charge jumps to the neighboring sites, it surmounts the potential barrier induced by the lattice deformation. Therefore, the hopping probability of the charge between the two sites is expected to be larger at higher temperature, and the strong electron−phonon coupling can cause the temperature dependence of the diffusion.

It should be notified that the lifetime of the neutral solitons was reported to be of the order of hours in the previous work, which was by several magnitudes longer than that in the present case.[20] The MX chain is considered to be partly disorder, and it is divided into the segmental areas.[24] When the soliton and

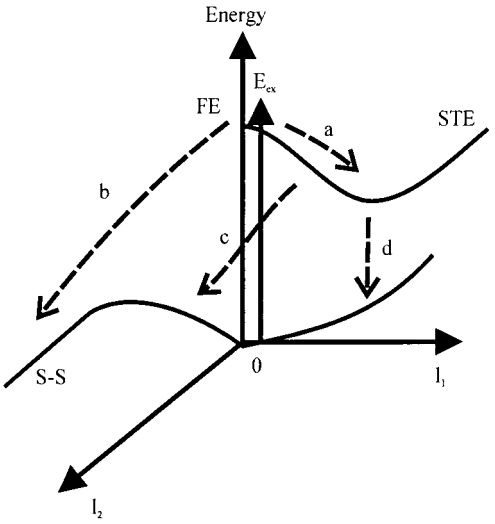

Figure 10. Adiabatic potential surface in a configuration space. l_1: coordinate of lattice relaxation associated with self-trapping process of exciton. l_2: soliton−antisoliton distance. G: electronic ground state. FE: free exciton. STE: self-trapped exciton. S−S: neutral soliton pair. a: thermalization of STE. b: lattice relaxation from FE to S−S. c: lattice relaxation from nonthermal STE to spatially confined S−S. d: relaxation of thermal STE.

antisoliton are distributed in the different segments, they have to surmount the potential barrier as high as 70 meV to recombine with each other.[20] The thermal activating process of the soliton is the reason for the long lifetime of the order of hours. On the other hand, when the soliton and antisoliton are occupied in the same segment, they will recombine without surmounting the potential barrier because of the disordered part in the MX chain. The kinetics of the PA signal seen in the present experimental result corresponds to the latter case.

Finally, the dynamics of the component C is argued, which is seen at the higher energy region of 1.9−2.6 eV. This excited state appears with a rise time τ_{C2} of about 1 ps, independent of the temperature, and disappears with a decay time of $\tau_{C1} = 3.4$ ps at 293 K and $\tau_{C1} = 8.8$ ps at 4 K, respectively. The rise time τ_{C2} is in good agreement with the thermalization time of the STE of $\tau_A = 880$ fs in eq 6. Thus, some portions of the nonthermal STEs are converted into the component C. In the previous work, it was demonstrated theoretically that the STE had a nonradiative lattice relaxation channel into the neutral soliton state. The case is different from the formation of the other nonlinear excitations, like charged soliton pair and polaron pair, because they are charged states and their formation is expected to come from an unbounded electron and hole pair. In other words, the exciton state without the charge should not be converted into the charged state, such as the charged soliton pair and polaron pair. Therefore, the component C may be attributed to the neutral soliton pair with a lattice configuration different from the component D, which was above-mentioned.

The difference in these two kinds of the neutral soliton pairs is explained with the previous theoretical work using the extended Peierls−Hubbard model.[31] In the model, it was claimed that the potential surface is continuous between the electronic ground and neutral soliton pair states as shown in Figure 10. The interaction is attractive between the soliton and antisoliton, when the pair distance is short in the vicinity of $l_2 = 0$ where their wave functions overlap with each other. In this case, the soliton pair should be effectively confined in this attractive potential. The hopping probability of the soliton toward the counterpart is larger than that against it. On the other hand, when the pair distance l_2 is large and the overlap of their wave functions is negligible, the potential surface is approximated to be flat. In this region, the hopping probabilities toward and against the counterpart are the same, and the soliton and antisoliton transport freely along the MX chain without suffering the interaction from the counterpart.

In the present experimental cases, the temporal profiles of the PA due to the component D is approximated with the function $\mathrm{erf}[(t/T_D)^{-1/2}]$, which expresses the geminate recombination process of the pair excited species along the ideal one-dimensional line. This means that the initial separation l_0 is sufficiently large and the pair species transport on the flat potential surface corresponding to large l_2 value in most of the delay times. Because the soliton pair is converted directly from the free exciton state, they have a sufficiently large excess vibrational energy to attain the large l_0 separation. On the other hand, the component C may be attributed to the soliton pair in the vicinity of $l_2 = 0$, and the soliton and antisoliton pair are attractive with each other, which results in the mutual spatial confinement. Because this confined state is generated by way of the vibrationally relaxed STE state, the soliton pair does not have enough excess energy to overcome the attractive potential. Furthermore, the probability of the geminate recombination is expected to be larger under the condition of the finite chain length, comparing with the kinetics in the infinitely long chain length, according to the previous work.[45] On the finite chain length, the solution of the diffusion equation is approximated to the exponential function rather than the equation expressed with the error function, as in the present case.

5. Conclusions

The time-resolved absorption spectrum is studied for the quasi-one-dimensional HMMC $[Pt(en)_2][Pt(en)_2Cl_2](ClO_4)_4$ with pump−probe spectroscopy. The transient absorption spectrum is measured throughout a broadband probe energy region of 0.6−2.6 eV, obtained by difference frequency generation. The contributions both from the absorption because of the STE and from the neutral-soliton pair are found in the broad absorption band. In the relaxation process of the STE, the nonequilibrated exciton is thermalized within 1 ps after the formation. For the neutral-soliton pairs, two different types of the geometrical configurations are observed: the spatially confined neutral-soliton pair and the spatially uncorrelated neutral-soliton pair. Among them, the spatially uncorrelated soliton pair is generated directly from the photogenerated free exciton state, whereas the specially confined neutral-soliton pair is from the STE state.

Acknowledgment. This work is supported by Research for the Future (RFTF) of Japan Society for the Promotion of Sciences. The authors thank Prof. S. Kurita and Prof. J. Takeda for many fruitful discussions. They thank Dr. H. F. Hofmann for his critical reading of the manuscript.

References and Notes

(1) Ueta, M.; Kanzaki, H.; Kobayashi, K.; Toyozawa, Y.; Hanamura, E.; *Excitonic Processes in Solids*; Springer-Verlag: Berlin, 1986; Chapter 4.

(2) Song, K. S.; Williams, R. T. *Self-Trapped Excitons*, 2nd ed.; Springer-Verlag: Berlin, 1996; Chapter 2.

(3) Kobayashi, T. *Relaxation in Polymers*; World Scientific: Singapore, 1993.

(4) Heeger J.; Kilveson, S.; Schireffer, J. R.; Su, W.-P. *Rev. Mod. Phys.* **1988**, *60*, 781.

(5) Kobayashi, T.; Yoshizawa, M.; Stamm, U.; Taiji, M.; Hasegawa, M. *J. Opt. Soc. Am.* **1990**, B7, 1558.

(6) Takeuchi, S.; Masuda, T.; Kobayashi, T. *J. Chem. Phys.* **1996**, *105*, 2859.

(7) Kobayashi, T. *J-Aggregate*; World Scientific: Singapore, 1996.

(8) Misawa, K.; Kobayashi, T. *J. Chem. Phys.* **1999**, *110*, 5844.
(9) Iwai, S.; Kamata, T.; Murata, S.; Fukaya, T.; Kodaira, T.; Mizukami, F., Tachiya, M.; Yamamoto, K.; Ohta, T. *J. Chem. Phys.* **1999**, *110*, 8687.
(10) Iwai, S.; Kamata, T.; Murata, S.; Yamamoto, K.; Ohta, T. *J. Chem. Phys.* **1999**, *111*, 5402.
(11) Wada, Y.; Mitani, T.; Yamashita M.; Koda, T. *J. Phys. Soc. Jpn.* **1985**, *54*, 3143.
(12) Wada, Y.; Mitani, T.; Toriumi, K.; Yamashita, M. *J. Phys. Soc. Jpn.* **1989**, *58*, 3013.
(13) Wada, Y.; Yamashita, M. *Phys. Rev. B* **1990**, *42*, 7398.
(14) Okamoto, H.; Mitani, T. *Prog. Theor. Phys. Suppl.* **1993**, *113*, 191.
(15) Nasu, K. *J. Phys. Soc. Jpn.* **1983**, *52*, 3865.
(16) Nasu, K. *J. Phys. Soc. Jpn.* **1984**, *53*, 302.
(17) Nasu, K. *J. Phys. Soc. Jpn.* **1984**, *53*, 427.
(18) Iwano, K.; Nasu, K. *J. Phys. Soc. Jpn.* **1992**, *61*, 1380.
(19) Tanaka M.; Kurita, S.; Okada, Y.; Kojima, T.; Yamada, Y. *Chem. Phys*. **1985**, *96*, 343.
(20) Kurita, S.; Haruki, M.; Miyagawa, K. *J. Phys. Soc. Jpn.* **1988**, *57*, 1789.
(21) Okamoto, H.; Mitani, T.; Toriumi, K.; Yamashita, M. *Phys. Rev. Lett.* **1992**, *69*, 2248.
(22) Okamoto, H.; Oka, Y.; Mitani, T.; Yamashita, M. *Phys. Rev. B* **1997**, *55*, 6330.
(23) Kuroda, N.; Wakabayashi, Y.; Nishida, M.; Wakabayashi, N.; Yamashita, M.; Matsushita, N. *Phys. Rev. Lett.* **1997**, *79*, 2510.
(24) Kuroda, N.; Tabata, Y.; Nishida, N.; Yamashita, M. *Phys. Rev. B* **1999**, *59*, 12973.
(25) Okamoto, H.; Kaga, Y.; Shimada, Y.; Oka, Y.; Iwasa, Y.; Mitani, T.; Yamashita, M. *Phys. Rev. Lett.* **1998**, *80*, 861.
(26) Wada, Y.; Matsushita, N.; Tanaka, J.; Mitsuhashi, T. *J. Lumin.* **1996**, *66/67*, 120.
(27) Kuroda, N.; Sakai, M.; Suezawa, M.; Nishina, Y.; Sumino, K. *J. Phys. Soc. Jpn.* **1990**, *59*, 3049.
(28) Mishima, A.; Nasu, K. *Phys. Rev. B* **1989**, *39*, 5758.
(29) Mishima, A.; Nasu, K. *Phys. Rev. B* **1989**, *39*, 5763.
(30) Suzuki, M.; Nasu, K. *Phys. Rev. B* **1992**, *45*, 1605.
(31) Iwano, K. *J. Phys. Soc. Jpn.* **1997**, *66*, 1088.
(32) Rashba, E. I.; Sturge, M. D. *Excitons*; North-Holland: Amsterdam, 1987.
(33) Wada, Y.; Lemmer, U.; Göbel, E. O.; Yamashita, M.; Toriumi, K. *Phys. Rev. B* **1995**, *52*, 8276.
(34) Ooi, H.; Yamashita, M.; Kobayashi, T. *Solid State Comm.* **1993**, *86*, 789.
(35) Dexheimer, S. L.; Pelt, A. D.; Brozik, J. A.; Swanson, B. I. *Phys. Rev. Lett.* **2000**, *84*, 4425.
(36) Kobayashi, T.; Sekikawa, T.; Yamashita, M. *Chem. Lett.* **1997**, 1029.
(37) Tomimoto, S.; Nansei, H.; Saito, S.; Suemoto, T.; Takeda, J.; Kurita, S. *Phys. Rev. Lett.* **1998**, *81*, 417.
(38) Kanner, G. S.; Strouse, G. F.; Swanson, B. I.; Sinclair, M.; Jiang, J. P.; Peyghambarian, N. *Phys. Rev. B* **1997**, *56*, 2501.
(39) Sugita, A.; Yamashita, M.; Kobayashi, T. *J. Chem. Phys.* **2001**, *114*, 2369.
(40) Matsumoto, N.; Yamashita, M.; Kida, S. *Bull. Chem. Soc. Jpn.* **1978**, *51*, 2334.
(41) Iwasa, Y.; Funatsu, E.; Hasegawa, T.; Koda, T.; Yamashita, M. *Appl. Phys. Lett.* **1991**, *59*, 2219.
(42) Tamura, K.; Ippen, E. P.; Haus, H. A.; Nelson, L. E. *Opt. Lett.* **1993**, *18*, 1080.
(43) Takeuchi, S.; Kobayashi, T. *J. Appl. Phys.* **1994**, *75*, 2757.
(44) Roessler, D. M. *Brit. J. Appl. Phys.* **1965**, *16*, 1119.
(45) Zozulenko, I. V. *Solid State Comm.* **1990**, *76*, 1035.
(46) Shank, C. V.; Yen, R.; Fork, R. L.; Orenstein, J.; Baler, G. L. *Phys. Rev. Lett.* **1982**, *49*, 1660.
(47) Nisoli, M.; Ottone, A. C.; De Silvestri, S.; Magni, V.; Svelto, O.; Tubino, R.; Botta, C. *IEEE J. Quantum Electron*. **1993**, *29*, 1006.
(48) Matsushita, N.; Kojima, N.; Watanabe, N.; Ban, T. *Solid State Comm.* **1989**, *71*, 253.